

applied optics

Dislocated spots and triple splittings of natural rainbows generated by large drop distortions, oscillations, and tilts

ALEXANDER HAUSSMANN

Arbeitskreis Meteore e.V., Schipkauer Straße 26, D-01968 Hörlitz, Germany (alexander.haussmann@web.de)

Received 28 February 2020; revised 30 April 2020; accepted 1 May 2020; posted 1 May 2020 (Doc. ID 391405); published 10 June 2020

For an accurate modeling of natural rainbows, it is necessary to take into account the flattened shape of falling raindrops. Larger drops do also oscillate, and their axes exhibit tilt angles with respect to the vertical. In this paper, I will discuss two rare rainbow phenomena that are influenced by these effects: bright spots belonging to various rainbow orders, but appearing at remarkable angular distances from their traditional locations, as well as triple-split primary rainbows. While the former have not been observed in nature so far, the latter have been documented in a few photographs. This paper presents simulations based on natural drop size distributions using both a geometric optical model, as well as numerically calculated Möbius shifts applied to Debye series data. © 2020 Optical Society of America

https://doi.org/10.1364/AO.391405

1. INTRODUCTION

Many of the well-known physical theories for the rainbow, or, more precisely, the whole sequence of multiple rainbow orders, hinge on the assumption that raindrops possess an exactly spherical shape. This includes geometric optics (Descartes), early wave optics (Young, Airy), and classical electrodynamics (Lorenz–Mie scattering and its decomposition into the Debye series, as well as complex angular momentum theory) [1]. However, falling raindrops are never truly spherical in shape, due to the interplay of surface tension, gravity, aerodynamic drag, internal circulation, and, if present, strong electrostatic fields. While quantitative measurements and modeling of these effects became possible only a few decades ago, the general observation that drops become flattened as they fall found its way into a few rainbow explanations surprisingly early, dating back to Maurolico (1553) and Marcus Marci (1648), both aiming at the reconciliation of their (wrong) theories with the observed angular size of the rainbow [2]. Later, Venturi (1814) discussed drops whose degree of oblateness increased with their size as an explanation for the then still enigmatic supernumerary arcs. While the competing wave-optical model became more and more accepted in the ensuing decades, Venturi had effectively provided the modern explanation for twinned rainbows [3].

In 1907, Möbius showed that for nearly spherical drops, the dominant effect is a mere shift of the rainbows, including their supernumerary pattern, to a different scattering angle [4]. This shift concept proved to be a useful starting point for the exploration of details in natural rainbow displays, such as the

visibility of supernumeraries in broad drop size distributions (DSDs) [5,6]. Consequently, the original Möbius formula, a first-order expansion in the drop ellipticity valid for the primary rainbow's top only, was generalized to account for all scattering azimuths (clock angles) around the primary and secondary rainbows' circumferences [7], and also higher-order rainbows [3]. Furthermore, also more advanced shape models that provide a better fit to natural drops can successfully be dealt with within the framework of such Möbius shifts [8], though for simulations, extensive lookup tables have to be created by numerical ray tracing beforehand [9,10]. However, even for the most accurate model shapes and low overall deformations, the Möbius shift still remains only an approximation. Deviations from it, manifesting as variations in the supernumerary spacing, have been calculated and measured [11,12].

A qualitatively different situation arises when the deviations from a sphere become more pronounced, which in natural rainfall happens for larger drops. Then, width and intensity of the respective rainbows (especially the higher orders) can vary strongly, and their position is changed so drastically that referencing to the spherical drops' rainbows in terms of a shift is not meaningful anymore. Moreover, additional and disjoint caustic features apart from the traditional fold caustic will appear. These are of fundamental interest as examples for optical catastrophe theory and have been studied in various single-drop laboratory experiments [13–17]. Another example is the "90° rainbow" identified in scattering calculations [18,19]. However, as of now there are no clear reports of such unusual bright spots or arcs at unexpected locations in natural rainbow displays. This is

caused by the inherent width of typical DSDs, which encompass considerable amounts of raindrops in a large range of sizes and, as a consequence, a large range of different shapes.

In order to check if any such natural superpositions of caustic features from distorted drops can become visible against the background in the field, it is thus necessary to simulate rainbows of multiple orders using broad DSDs that also contain a significant amount of larger drops (sphere-equivalent radius $> \approx 0.8$ mm). Thereby, effects that are stable with respect to natural drop shape variations can be identified. As it turns out, such "stable superpositions" do indeed exist, and they take the appearance of bright spots in the Sun's vertical at considerable angular distances from the traditional locations of the corresponding rainbow orders. Furthermore, it is well known that larger raindrops are prone to shape oscillations. The mechanical theory of drop oscillations is worked out to a high degree; however, the question which oscillation modes dominate for which drop size in natural rain is still under debate [20]. In fact, rainbow scattering has been used as an optical tool for determining oscillation frequencies and modes [21,22]. The main difference between such single-drop experiments and natural rainbows is, however, that in the former the effect of individual elongation states on the rainbow-scattered light can be monitored, either by temporally resolving the drop as it falls [23], or by streak photography [8,21,22]. For natural bows, only the spatial and temporal average over many drops and usual exposure times matters for the overall impression, though occasionally individual oscillation streaks from nearby drops can be photographed in sunlight (see [24], Section 1). For the simulations, I will assume that the oscillations have random phases, though it is also possible that sudden changes in the electrostatic field (lightning) or sound waves (thunder) can synchronize drop oscillations for some time. There are, in fact, very few older observations of thunder influencing rainbows [8], but I am not aware of any modern records of such phenomena.

Drop oscillations can also be responsible for the very rare primary rainbows, which split up into three branches, a situation that is clearly distinct from a pattern of supernumerary arcs and at first glance seems to be a more extreme case of rainbow twinning. A few of these have been photographed in past years, and their analysis reveals that one of the branches extends into Alexander's dark band [25–28]. This is the opposite direction of the usual Möbius shift, and can only be accounted for by improbably high deviations of the drop axes from the vertical, or elongated drop shapes. Drops may become elongated due to electrostatic fields that might be present under thunderstorm clouds [29], or, as will be discussed here, elongated states exist temporarily during the course of axisymmetric oscillations.

Finally, it has to be taken into account that the raindrops' axes will not be oriented strictly vertically, but exhibit a statistical distribution of finite width similar to the axes of ice crystals in halo phenomena [30]. Experimental data for the (likely also size-dependent) distribution of axis tilt angles is only scarcely available [31,32]. Nonetheless, the effect of these tilts on the bright spots and triple-split rainbows will also be discussed.

2. THEORETICAL BACKGROUND

A. Simulation Methods

Over the past few years, several studies have addressed the problem of true color simulations of rainbows [33–36]. In this paper, I will use two simulation methods: 1) geometric optic ray tracing, taking into account polarization but neglecting interference (GO), and 2) applying Möbius shifts to intensity data for various rainbow orders calculated using the Debye series, i.e., the electrodynamic solution of the scattering problem for spheres. The use of shifts for all clock angles around the full circumference of the rainbow, and the extension of the concept to orders higher than the primary, was pioneered by Können [7]. Therefore, I will refer to this method as Debye–Möbius–Können (DMK).

These methods represent complementary approximation domains. GO is robust with respect to drop shapes, but is not able to reproduce supernumerary bows. The main obstacle for the inclusion of interference effects are phase shifts that occur when rays pass focal lines. This effect has been studied for spherical drops in great detail [37,38], but there seems to be no simple method to determine the location of focal lines in distorted drops. DMK, on the other hand, will give proper supernumeraries, but is limited to small shape deviations from the spherical reference. Both methods are discussed in more detail in a previous publication, which mainly addressed polarization effects and higher order rainbow twinning [10,39]. As in the earlier simulation study, I will neglect effects from the scattering geometry and multiscattering [34,40], allowing one to interpret the properly summed scattering outputs of single model drops as the rainbows seen by an observer or camera. The spectrum of the high Sun is used for all calculations, as well as the spectral response of a Pentax K-5 camera for color space mapping. The Sun's angular diameter is set to 0.54°. I will also concentrate exclusively on the resulting intensity sum as seen by a polarization insensitive detector here.

For the purpose of this paper, I extended the GO calculations up to seven internal reflections in the modeled drop, as, apart from observations up to the first five rainbow orders, there is also a report on the possible detection of the seventh order in nature [41]. Moreover, scattering features belonging to the sixth order might become intensified to a degree that allows their detection against the primary's background [13], though this is not to be expected for spherical drops [42]. Rather bright sixth-order caustics from single drops, deformed by their own weight when resting on ultrahydrophobic supports, have indeed been observed [17]. DMK simulations are carried out for the primary and secondary rainbows in a limited drop size range only, as they are used exclusively for the discussion of the specific phenomenon of triple-split bows. In order to match the statistic distributions of oscillation phases and tilt angles, at each simulation pixel individual pseudo-random values for these parameters were generated according to the respective probability density. To smoothen the final results, several (typically 16) of these Monte Carlo simulation runs were subsequently averaged.

B. Equilibrium Drop Shapes

A variety of models has been proposed to describe the equilibrium (i.e., nonoscillating) shape of falling raindrops. The first logical step away from spheres are oblate spheroids, as originally treated by Möbius (though not in the context of actual raindrops), and numerous subsequent studies. They bear the advantage of allowing one to derive analytic approximations for the Möbius shift [3,4], and even exact electrodynamic solutions of the scattering problem [43,44]. I will refer to this model as "1S" (one spheroid). In order to account for the observed asymmetry between the upper and the lower parts of the drop, this model can be modified by assigning different degrees of oblateness to these parts ("2HS" = two half-spheroids) [9,10,45,46]. A further refinement is possible by dividing the lower part again into two spheroids, one with a shifted center ("3PS" = three partial spheroids) [17]. Alternatively, the center distance r_0 of the drop's outline in an arbitrary vertical cut through the center can be expanded into a cosine series of the polar angle ϑ [47]

$$r_0\left(\vartheta\right) = a_0 \cdot \left(1 + \sum_{n=0}^{n_{\text{max}}} c_n \cdot \cos\left(n \cdot (\pi - \vartheta)\right)\right). \tag{1}$$

In this equation, the parameter a_0 corresponds to the radius of a sphere with the same volume ("equivalent radius"), and I chose to change the $\vartheta = 0$ direction to the positive z axis here, in contrast to the original definition in Ref. [47]. The deformation is described by the set of coefficients c_n .

By construction, the surface curvature is continuous at any point for this model, which is not the case for the stitched 2HS and 3PS shapes. Moreover, values for the relevant c_n up to $n_{\rm max}=10$ for the widely applied physical drop model of Beard and Chuang [48] (balancing the effects of surface tension as well as hydrostatic and atmospheric pressures in the Young–Laplace equation) are readily available for selected drop sizes. Therefore, this model will be adopted for all GO simulations in this paper (abbreviated "BC"). From the data set published in [49], I interpolated c_n values for 80 drop sizes in the range of $a_0=0.025$ mm to $a_0=2$ mm (see [24], Section 2 for mathematical details).

The disadvantage of this model is the higher numerical effort, as all intersection points of light rays with the surface have to be calculated by iteration rather than by closed formulas as in the case of spheroid-based models. Though it is possible to use the BC model also for the calculation of a Möbius shift lookup database for DMK simulations, limited computational resources made it necessary to resort to older 2HS data for the purpose of this paper. This is acceptable, as in the case of triple-split bows only drop sizes below $a_0 < 1$ mm with moderate shape distortions are relevant. Sample calculations for a drop size of $a_0 = 0.5$ mm show a sufficient consistency between the two models (see [24], Section 3). Formulas for the 2HS parameters designed to fit best to the BC model can be found in Refs. [9,50]; also, the inclusion of (2,0) oscillations is comparatively easy.

C. Raindrop Oscillations

In the absence of external forces, the equilibrium shape of a drop of incompressible fluid is a sphere of a certain radius, thus

minimizing its surface area and occupying the energetic minimum of the oscillator potential created by the surface tension. A disturbance of this shape will result in oscillations around this equilibrium, damped by internal friction due to the fluid's viscosity. In the regime of small amplitudes (i.e., a linearized model), the normal modes (or eigenmodes) of such a drop are real-valued spherical harmonics (i.e., proper linear combinations of the complex spherical harmonics conventionally used in quantum mechanics, etc.). Also, for slightly oblate drops, such as natural raindrops, spherical harmonics are a suitable basis function system to describe their small-amplitude oscillations, and it can be assumed that they still match the normal modes reasonably well. The direction-dependent local drop radius r (distance from the center) is given by [22,51,52]

$$r(\vartheta, \varphi, t) = r_0(\vartheta) + \sum_{l=2}^{\infty} \sum_{m=-l}^{l} A_{l,m}$$

$$\cdot \sin(\omega_{l,m} \cdot t + \psi_{l,m}) \cdot Y_{l,m}(\vartheta, \varphi).$$
 (2)

This formula describes a superposition of real-valued normalized spherical harmonics $Y_{l,m}$ (see [24], Section 2) with amplitudes $A_{l,m}$, (angular) frequencies $\omega_{l,m}$, and phase offsets $\psi_{l,m}$, which is added to the equilibrium radius r_0 . Oscillation modes start at l=2 with the so-called quadrupolar modes, as the l=0 term would contradict volume conservation and l=1 corresponds, in the small amplitude approximation, only to a translation of the whole drop. The frequency spectrum of a spherical drop, first derived by Rayleigh (1879), is given by

$$\omega_l = \sqrt{\frac{\sigma \cdot l \cdot (l-1) \cdot (l+2)}{\rho \cdot a_0^3}}.$$
 (3)

Note that for a fixed l, all modes for various m exhibit the same frequency [53]. This degeneracy is lifted for nonspherical equilibrium shapes [20,54], leading to slightly different frequencies $\omega_{l,m}$ and a beating effect in temporally resolved axis-ratio measurements of individual drops in multimode oscillation states [55]. The surface tension for water at 20°C amounts to about $\sigma = 0.073 \, \mathrm{Jm}^{-2}$ (at a density of $\rho = 998 \, \mathrm{kgm}^{-3}$), though there can be deviations for drops containing impurities [56]. The 1/e damping time is, under several realistic assumptions [51,55],

$$\tau_l = \frac{\rho \cdot a_0^2}{\eta \cdot (l-1) \cdot (2l+1)}.$$

At 20°C, the dynamic viscosity of water amounts to about $\eta = 0.001 \, \text{Nsm}^{-2}$. This results in typical values of $T = 2\pi/\omega = 3 \, \text{ms}$ and $\tau = 50 \, \text{ms}$ for a drop of $a_0 = 0.5 \, \text{mm}$ oscillating in a (2, m), i.e., quadrupolar, mode. For larger amplitudes $(A_{l,m} > \approx 0.1 a_0)$, nonlinear effects have to be taken into account [51].

As seen, the damping increases with l, leading to the expectation that the low modes will be most important. Typically, with increasing drop size, an onset of noticeable oscillations is observed at about $a_0 = 0.5$ mm, with rising amplitudes as the drops get larger. Possible effects that constantly reinstigate the oscillations are resonant back actions from the eddy shedding

in the drop's rear, wind shear, and turbulence, and collisions between drops [57]. Because of this multitude of influences and experimental challenges in mode analysis, it is yet not fully clear which exact modes will be typically encountered at which drop size in natural rain. From measurements, the occasional presence of (2,0), (2,1), (2,2), and (3,1) modes has been inferred [20].

D. (2,0) Mode

Because of the ambiguity concerning the relevant modes, I decided to start with the simplest case, the fundamental axisymmetric (2,0) mode. For this, the local drop radius is given by

$$r(\vartheta, t) = r_0(\vartheta) + a_0 \cdot A_{2,0}^* \cdot \sin\left(\omega_{2,0} \cdot t + \psi_{2,0}\right)$$
$$\cdot \left[\frac{1}{2} \cdot \left(3\cos^2\vartheta - 1\right)\right]. \tag{5}$$

 $A_{2,0}^*$ was redefined with respect to Eq. (2), being now a dimensionless relative amplitude (and absorbing the normalization factor between the Legendre polynomial P_2 and the spherical harmonic $Y_{2,0}$ (see [24], Section 2). Luckily, trigonometric relations allow the conversion of Eq. (5) into the cosine series of Eq. (1) by changing only two of the coefficients:

$$c_0^* = c_0 + \frac{1}{4} A_{2,0}^* \cdot q \quad c_2^* = c_2 + \frac{3}{4} A_{2,0}^* \cdot q.$$
 (6)

Here, $q=\sin(\omega_{2,0}\cdot t+\psi_{2,0})$ represents the time-dependent oscillation state. Figures 1(a)-1(c) show, for illustration, the extremal negative (q=-1), zero (q=0), and extremal positive (q=+1) elongation state for an $a_0=1.5$ mm BC model drop at a (somewhat exaggerated) amplitude of $A_{2,0}^*=0.15$. In order to reproduce the desired case of a temporal and desynchronized ensemble mean, for each ray candidate (total number, typically $1\dots 6\cdot 10^6$) an individual oscillation state is chosen according to $q=\sin(2\pi\cdot x)$, with a pseudo-random number x between 0 and 1 from a uniform distribution.

Typical results of oscillation measurements are axis ratios, i.e. the quotients of vertical and horizontal dimensions of the drops. In the case of a purely single-mode (2,0) oscillation, the axis ratio ξ in an elongated state in comparison to the equilibrium shape axis ratio $\bar{\xi}$ [58] for nearly spherical drops is related to the elongation $A_{2,0}^* \cdot q$ the following way:

$$\xi - \bar{\xi} \approx \frac{3}{2} A_{2,0}^* \cdot q. \tag{7}$$

For a more precise conversion, a lookup table was calculated numerically (see [24], Section 2 for a graphical representation). As a somewhat justified starting point for the size dependence of amplitudes, I used a data fit from a vertical wind tunnel experiment, carried out by Szakáll *et al.* in Mainz [20],

$$\xi_{\text{max}} - \xi_{\text{min}} = 0.0036 \cdot \left(2 \cdot \frac{a_0}{1 \text{ mm}}\right)^2 + 0.0213 \cdot \left(2 \cdot \frac{a_0}{1 \text{ mm}}\right).$$

The size-dependent amplitudes, under the assumption that only the (2,0) mode is active, can be calculated using the lookup

table and fitted to a third-degree polynomial,

$$A_{2,0}^* = 0.001133 \cdot \left(\frac{a_0}{1 \text{ mm}}\right)^3 + 0.004776 \cdot \left(\frac{a_0}{1 \text{ mm}}\right)^2 + 0.01407 \cdot \left(\frac{a_0}{1 \text{ mm}}\right).$$
 (9)

The (2,0) mode is also easily integrated in the 2HS model used for the calculation of Möbius shifts. The formulas in [9] provide a description in terms of the mean equilibrium axis ratio $\bar{\xi}$ and an asymmetry parameter $\Delta \xi$ representing the difference in vertical extent of the upper and lower part. Due to the symmetry of the (2,0) mode, it is justified to adjust only $\bar{\xi}$ according to the present elongation by using the lookup table, while keeping $\Delta \xi$ fixed. Again, the general consistency with the BC model was checked for selected cases (see [24], Section 3).

A key feature of the (2,0) mode is its inherent selection effect. As the momentary velocity of a mechanical oscillator reaches zero at its turning points, chances are higher of encountering states close to the turning points when randomly checking on it. The probability density of encountering an oscillation state $-1 \le q \le 1$ is

$$\frac{dP}{dq} = \frac{1}{\pi \cdot \sqrt{1 - q^2}}.$$
 (10)

This is illustrated in a numerical experiment shown in Figs. 1(d) and 1(e): For a single, precisely fixed amplitude (d), a histogram over the elongations (e) shows the behavior predicted by Eq. (10) (the singularities at the turning points are not critical for any finite bin width). This means that a single drop size can effectively contribute with two relevant shapes to the rainbow, instead of only one, as previously assumed [9,10].

The situation becomes more complex when taking into account that in a large ensemble not all drops will exhibit the same (=monodisperse) oscillation amplitude. As most measurements focus on single drops, there are no reliable data describing the natural spread of polydisperse amplitudes. As a first guess, I chose a Gaussian distribution with a relative standard deviation of $\sigma_{\rm rel}=0.3$ around the previously used monodisperse value [Fig. 1(f)]. This results in a much more smeared-out elongation histogram [Fig. 1(g), being essentially the convolution of 1(e) and 1(f)].

E. Drop Axis Tilts

BC equilibrium shapes, as well as BC drops in (2,0) oscillations, still possess a symmetry axis, which in the undisturbed case is expected to coincide with the vertical. However, as known from ice crystal halos [30], finite tilt distributions may occur. For raindrops, there are a few theoretical analyses [59] and experimental studies [31,32] on this effect. In the reported experiment, artificially generated drops of $a_0 = 1...4$ mm were imaged after an 80 m fall under calm conditions. The results were consistent with a Gaussian distribution on the direction sphere [Fig. 1(h)], with standard deviations of $\sigma = 7^{\circ} ... 8^{\circ}$. The corresponding probability density for drop tilt angles ϑ_D is

$$\frac{dP}{d\vartheta_D} = N \cdot \sin(\vartheta_D) \cdot \exp\left(-\frac{\vartheta_D^2}{2\sigma^2}\right), \tag{11}$$

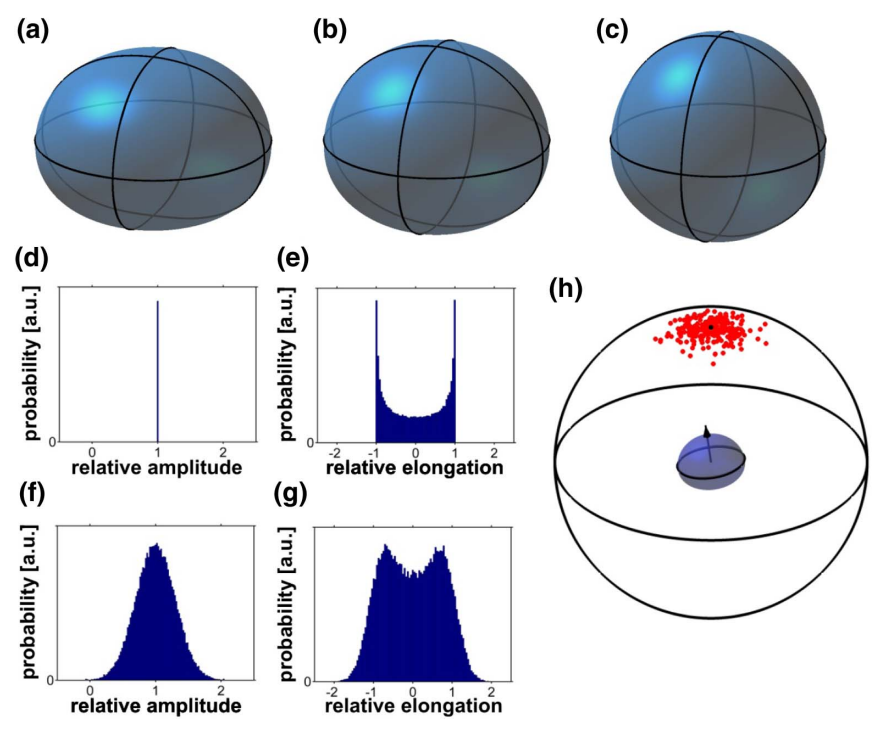


Fig. 1. (a) Extremal negative, (b) zero, and (c) extremal positive elongation of the (2,0) mode for an $a_0 = 1.5$ mm BC model drop at relative amplitude of $A_{2,0}^* = 0.15$; (d) monodisperse amplitude distribution from a numerical experiment involving 10^5 random (2,0) oscillation states; (e) corresponding elongation distribution, following Eq. (10); (f) Gaussian amplitude distribution with a relative standard deviation of 0.3; (g) corresponding elongation distribution; (h) Gaussian distribution of drop axis directions around the vertical (standard deviation 7° , 250 samples).

with a normalization factor N. Note the additional $\sin(\vartheta_D)$ factor that corrects for the mapping between intervals in ϑ_D and the actual solid angle region on the sphere. For the simulations, I chose a constant value of $\sigma=7^\circ$ for all drop sizes and uniformly distributed drop axis azimuths φ_D between 0° and 360° . For the resulting coordinate transformation matrix, see [24], Section 2.

Throughout this paper, I will assume that these moderate tilt angles do not affect the equilibrium drop shapes as described by the BC model. However, for larger amounts of canting caused by shear winds, the noncollinearity of aerodynamic drag and gravity will certainly lead to shape changes. It might also be argued that the oscillation behavior of tilted drops can differ from that of nontilted ones. However, according to finite-element simulations for falling drops, this seems not to be the case [60,61].

F. Drop Size Distributions

Many measured DSDs (number of drops per volume and size interval) can be fitted well with a gamma distribution using the parameters μ and Λ (n_0 is a normalization constant that cancels out when the simulation results are rendered as true-color images) [62],

$$n(a_0) = n_0 \cdot (2a_0)^{\mu} \cdot \exp(-\Lambda \cdot 2a_0).$$
 (12)

Such measurements usually rely on ground-based disdrometers. In contrast, the rainbow is not a spatially localized phenomenon, combining contributions from different regions of a sunlit shower along each viewing direction. In the single scattering limit, these contributions simply add up until the line of sight reaches the end of the shower, the end of the illuminated region, or the ground [9]. In dense showers, the situation is more complex [34,40]. I will use the term "effective DSD" (eDSD) here, in order to stress the difference from a spatially local property.

For the large drop GO simulations in this paper, I chose the parameter combination $\mu=1$ and $\Lambda=3$ mm⁻¹ (see Fig. 2, full line). An important fact to note is that the impact of a certain drop size on the rainbow is not given by the eDSD directly, but by the eDSD weighted with the scattering cross section of a single drop of this size (CS-eDSD, Fig. 2, dashed line). From such graphs, the dominant drop sizes are immediately recognizable. In geometric optics, the differential cross section of a sphere in the rainbow direction is proportional to a_0^2 ; in Airy theory, it is proportional to $a_0^{7/3}$ [1], which is only a minor difference. For consistency reasons, I chose the a_0^2 scaling here for all CS-eDSD graphs. In DMK simulations, I used $\mu=0$ and $\Lambda=4$ mm⁻¹, with the optional addition of narrow Gaussian peaks as previously applied in simulations of twinned rainbows [9,10].

Finally, the introduction of size-dependent oscillation amplitudes makes it necessary to further evolve the idea of the eDSD towards a 2D density depending now both on effective radius and (2,0) amplitude. This "effective drop size and oscillation amplitude density" (eDSOD) allows for instructive plots in the case of amplitude distributions with varying absolute standard deviation [see Fig. 4(i)] or even bimodal amplitude distributions [Figs. 6(a) and 6(b)]. For the discussion of multiple modes or size-dependent tilt distributions, more dimensions can still be

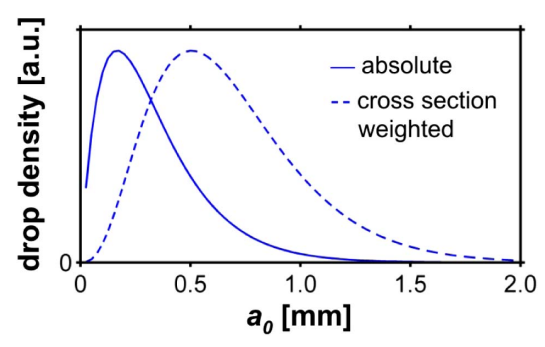


Fig. 2. Gamma-type DSD according to Eq. (12) for $\mu = 1$ and $\Lambda = 3 \text{ mm}^{-1}$, including a significant portion of larger drops. Cross section weighting was achieved by the multiplication with a_0^2 , as valid in the geometric optics regime. This eDSD was used for the GO simulations (Figs. 3 and 4).

added to the drop density concept. This illustrates the unexpected complexity of a rainbow "cooking recipe," even under the neglect of rain shower and shadow geometry, as well as the optical density of the illuminated assembly of drops.

3. RESULTS AND DISCUSSION

A. Bright Spots from Superposed Caustics in Broad eDSDs

The possible existence of new features in natural rainbows due to the more complex caustic structure of nonspherical drops was hinted at already more than two decades ago [15], also with regard to higher-order rainbows [16,18]. It was also noted that the instability of these features against shape variations is a critical issue for their detectability, due to the broadness of natural eDSDs [19]. The first aim of my investigations was therefore the identification of stable features. To do so, I carried out GO simulations using the $\mu = 1$, $\Lambda = 3 \text{ mm}^{-1}$ eDSD, but at first for zero oscillation amplitudes and zero tilts. I closely scrutinized the simulation results for the Sun elevation range $h_S = 0^{\circ} \dots 90^{\circ}$ (at 2° increments), leaving negative source elevations aside for the moment, as they are not important for natural bows [65]. However, subhorizon rainbow features were not rejected, as they might be seen from mountains, towers, airplanes, etc., or with the help of quadcopters.

I could indeed identify several concentrations of light created by nontraditional distorted-drop caustics of the second, fourth, fifth, sixth, and seventh rainbow order each, which have at least some chance to stand out against the background, or could possibly be extracted by similar image-processing methods as used for higher-order rainbows [66,67]. They all have the appearance of bright spots located in or near the Sun's vertical (0° or 180° in azimuth) and are dislocated with respect to their associated sphere drop rainbows. The left column of Fig. 3 shows simulations for the sum of all rainbow orders (up to the seventh), including external reflection and direct transmission through the drop (sometimes referred to as "zeroth order"). This corresponds to the impression seen by an observer or camera under optimal conditions, i.e., without external cloud or sky background. The middle column shows only specific rainbow orders, in order to highlight the feature in question. Of course,

such an effective filtering is not possible in nature. The bright spot of the fourth order (at $h_S = 60^\circ$) was not included in Fig. 3 because it appears only about 20° below the Sun and will therefore have the least chance to be detected against the intrinsic background (see [24], Section 4).

In the strict sense, these bright spots do not qualify as caustics themselves, as they are the result of an incoherent superposition of contributions from many drops, properly weighted by the CS-eDSD. True caustics can, however, be evaluated for each individual drop size involved. It turns out that for each spot at its optimal Sun elevation, there is a certain critical drop size for which the distorted and displaced rainbow caustic starts to involute by going through a cusp-like state. An example for this process is given in Ref. [24], Section 5. This "dominant drop size" produces the most concentrated and intense contribution to the spot (details of the intensity weighting are, however, influenced by the shape of the CS-eDSD). The corresponding ray paths are displayed in the right column of Fig. 3. As seen, total internal reflections-impossible for spheres-also play an important role in enhancing the intensities of the spots [17,45]. The individual drops' caustics are indeed colored, but most of the color is lost in the superposition. Also, for the cases of the second and sixth order, there exist associated "twin spots" of similar appearance caused by the reversed ray paths. These occur at solar elevations of $h_S = 6^{\circ}$ (second order, spot deep below the antisolar point) and $h_S = 36^{\circ}$ (sixth order—visible below the antisolar point in Fig. 3(a), and also for the slightly lower sun elevation of $h_S = 32^\circ$ in Fig. 3(j) and 3(k)) (see [24], Section 4).

At $h_S = 28^\circ$, the "subsun"-like spot of the fifth order [Fig. 3(h)] is accompanied by a "subparhelic circle" from directly transmitted rays [Fig. 3(g)]. This is the only new feature from the zeroth-order ray paths I could identify; otherwise, they just produce the familiar featureless bright forward-scattering disc. It has also to be noted that, with the exception of the second-order spot at $h_S = 36^\circ$ and the seventh-order spot at $h_S = 32^\circ$, all of the discussed features lie either below the horizon or are hidden in the zeroth-order disc, which makes their detection difficult. Indeed, I am not aware of any matching reports of such spots from natural displays [68,69].

Furthermore, the rudimentary traces of the lateral cusp caustics predicted for the first [15] and third order [16] for 1S drops and near-horizontal incidence appear in the Sun elevation simulation series (see [24], Section 6), modified according to the shape difference between the BC drops and the original up/down symmetric drop model, and washed out by the eDSD, so that only subtle parhelia-like enhancements remain. There is also a tendency for the rainbows to become diffuse in certain clock angle intervals for certain Sun elevations, due to the superposition of caustics whose positions strongly depend on the drop shape and which are fanned out accordingly. For instance, this affects the first and fifth orders for $h_S > \approx 30^\circ$ in the celestial region about 90° under the Sun (deep below the horizon). Precisely these two orders were discussed as contributors to a "90° rainbow" arc by Nousiainen et al. [18,19]. However, the vulnerability of any defined arc against changes in the drop shape was already noted in their papers. The present simulations did indeed confirm this statement.

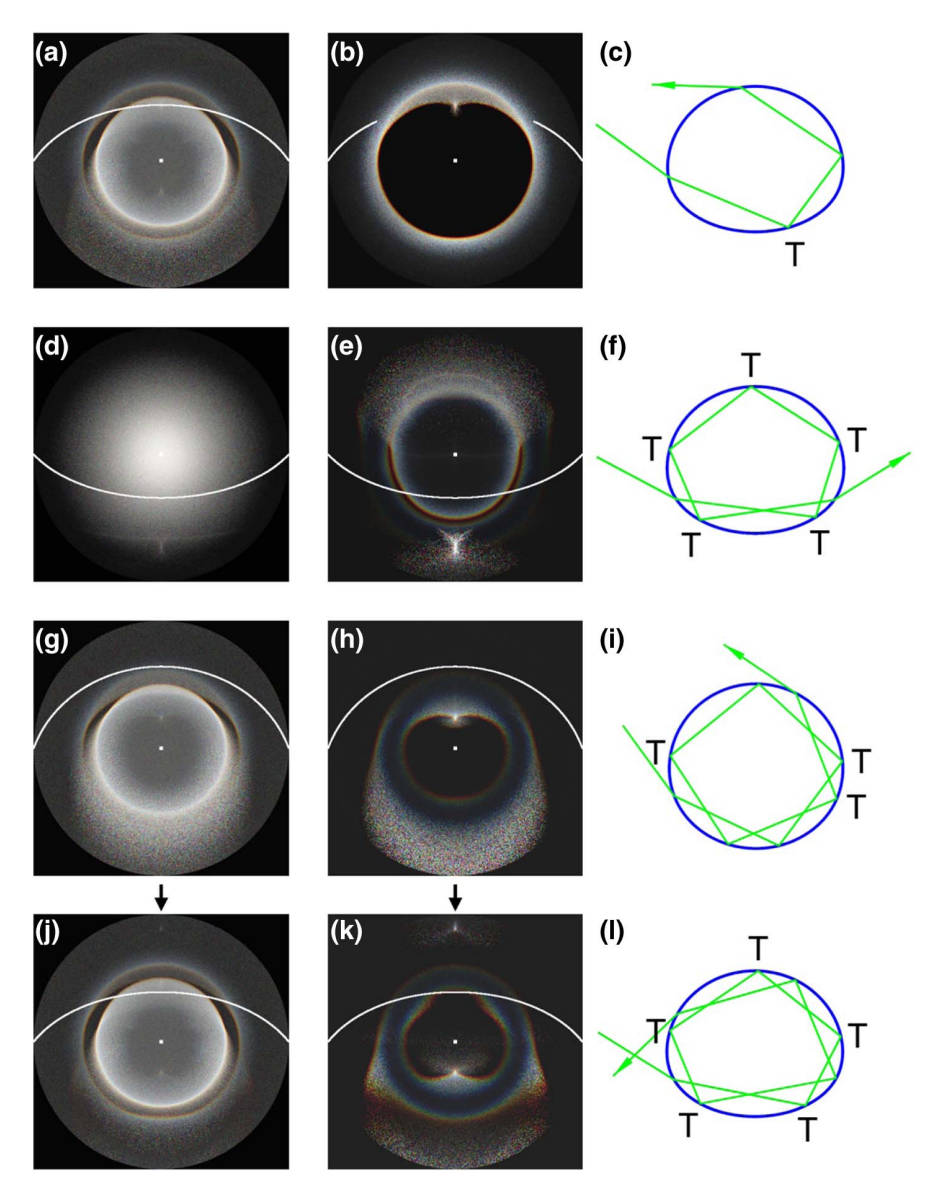


Fig. 3. GO simulations of dislocated bright spots from a $\mu=1$, $\Lambda=3$ mm⁻¹ eDSD without oscillations and at zero tilts. Equal-area (Lambert) projections encompassing one hemisphere are shown, with either the Sun or antisolar point in the center (white squares). The white line indicates the horizon. The right column depicts the responsible dominant ray paths for n=1.335 (green light). "T" denotes a total internal reflection. Bright spot from the second order, antisolar hemisphere, $h_S=36^\circ$: (a) all orders, (b) only second order, (c) ray path for $a_0=1.6$ mm. Bright spot from the fifth order, sunward hemisphere, $h_S=28^\circ$: (d) all orders, (e) only third–seventh order, (f) ray path for $a_0=1.6$ mm. Bright spot from the sixth order, antisolar hemisphere, $h_S=54^\circ$: (g) all orders, (h) only third–seventh order, (i) ray path for $a_0=0.8$ mm. Bright spot from the seventh order (marked by the arrow), antisolar hemisphere, $h_S=32^\circ$: (j) all orders, (k) only third–seventh order, (l) ray path for $a_0=1.6$ mm [63].

B. Bright Spots Versus (2,0) Oscillations and Tilts

I chose the near-horizon bright spot of the secondary as an example to study further to which extent it will be disturbed by oscillations and/or tilts. The results are summarized in Fig. 4. The first row shows the situation for zero tilts. As seen, the spot is elongated to a vertical pillar extending above the horizon, but does not lose its definition in the azimuthal direction, neither for monodisperse nor polydisperse amplitudes (both following the assumed "standard case" of Eq. (9); see the corresponding CS-eDSODs in the last row). This changes when Gaussian tilts (at $\sigma = 7^{\circ}$) are switched on (second row of Fig. 4): For each oscillation case, the bright spot is wiped out by the tilts. The

other spots from Fig. 3 show a similar behavior. Hence, the tilts are the key element deciding upon the visibility of such spots, at least as long as no other oscillation modes are involved.

C. Triple-Split Primary Rainbows

In contrast to the bright spots, primary bows splitting up into three branches have already been documented in nature beyond any doubt [see Fig. 5(a)] [25–28]. Nonetheless, they are rare, and so far, the few available reports stem from subtropic or tropic regions only. Compared to the bright spots, their explanation relies on much lower drop deformations. Therefore, they can be consistently attributed to smaller drops ($a_0 < 1 \, \text{mm}$), and a

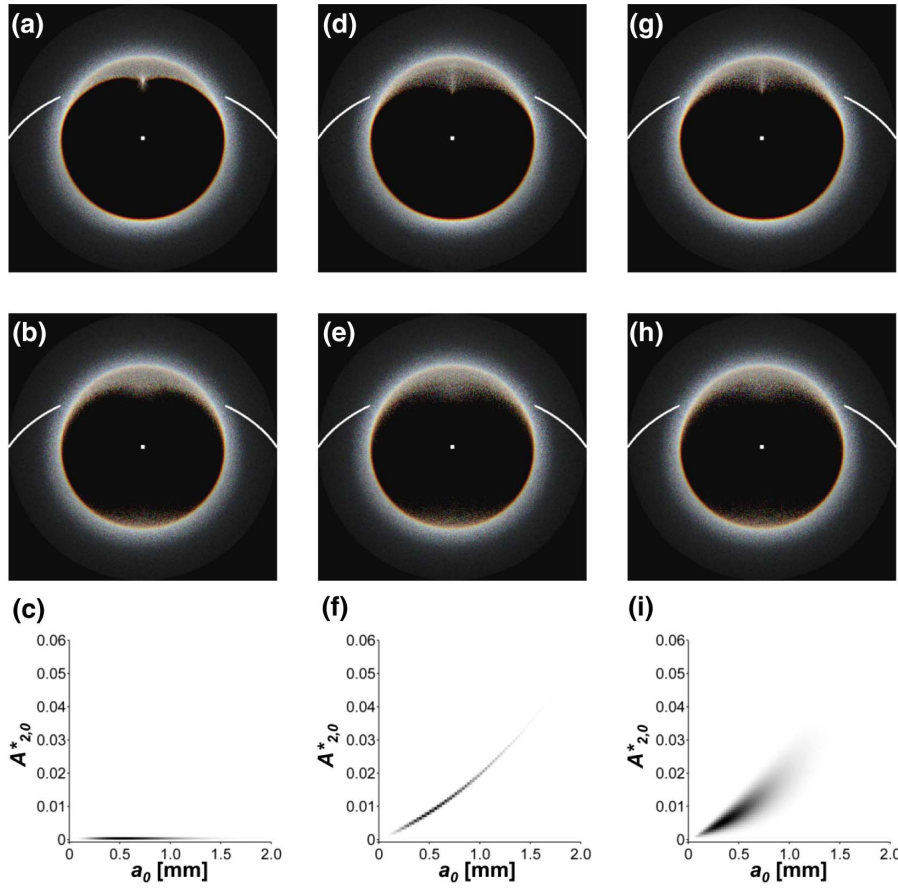


Fig. 4. Influence of (2,0) oscillations and Gaussian tilts on the second-order bright spot, $h_S = 36^\circ$. (a) Zero oscillations, zero tilts; (b) zero oscillations, tilts $\sigma = 7^\circ$; (c) corresponding CS-eDSOD; (d) monodisperse amplitudes according to Eq. (9), zero tilts; (e) monodisperse amplitudes, tilts $\sigma = 7^\circ$; (f) corresponding CS-eDSOD; (g) polydisperse amplitudes with $\sigma_{rel} = 0.3$, zero tilts; (h) polydisperse amplitudes with $\sigma_{rel} = 0.3$, tilts $\sigma = 7^\circ$; (i) corresponding CS-eDSOD. Color scaling for the CS-eDSODs runs from white to black, i.e., the darker a point, the higher the corresponding density of drops.

treatment within the approximative framework of Möbius shifts is appropriate.

Precise angular measurements of such photos are of great interest and in principle feasible [9,63], but require a careful calibration of the optical system and accurate position data from local reference points. For two specific cases, I mapped the photos into the scattering coordinate system (scattering angle, clock angle) as precisely as possible, relying on the information provided by the photographers [26,28] (one of these cases is shown in Fig. 5(a); for the other and for the reprojections in scattering coordinates, see [24], Section 7). Also, the secondary rainbow can be used as a position reference, as its visible part is, for usual Sun elevations, much less influenced by the comparatively low shape deformations in this drop size regime [10] (see also [24], Section 3). The secondary's arc above the horizon has not been observed to split up so far, either in nature or in the simulations [70].

From the analysis, it is almost certain that the upper branch of the split primary is shifted into Alexander's dark band (i.e., towards the secondary beyond the position of the sphere drop primary), at least in the two investigated cases. In contrast to this, the more frequent twinned rainbows can be consistently attributed to an additional peak at around $a_0 \approx 0.5$ mm in

the eDSD, which selects a narrow range from the continuously downward-shifted caustics from larger drops in order to create the lower branch. For oblate drops, the primary's Möbius shift is always directed towards the antisolar point for the arc above the horizon and Sun elevations that permit the visibility of such an arc $(h_S = 0^\circ \dots 42^\circ)$ [10] (see also [24], Section 3). This means that either improbably high tilts, narrowly centered around a preferred axis direction way off the vertical (see [24], Section 8), or elongated drops are needed to shift a primary rainbow upwards. It seems unlikely that even strong shear winds will topple over all the drops to the side in a coordinated manner. However, the consequences of such a situation cannot be predicted with absolute certainty from the current models based on BC drop shapes, as drops exposed to strong shear winds will exhibit different equilibrium shapes (see Section 2.E). Elongated shapes, on the other hand, require either additional forces such as electrostatic fields [29] or oscillations. I decided to test the latter possibility for the (2,0) mode in DMK simulations.

For this, I used an eDSD containing smaller drops ($\mu = 0$, $\Lambda = 4 \text{ mm}^{-1}$), a drop size cutoff at $a_0 = 1 \text{ mm}$, and a previously calculated Möbius shift database for 2HS model shapes. It is not surprising that under these conditions, the amplitude





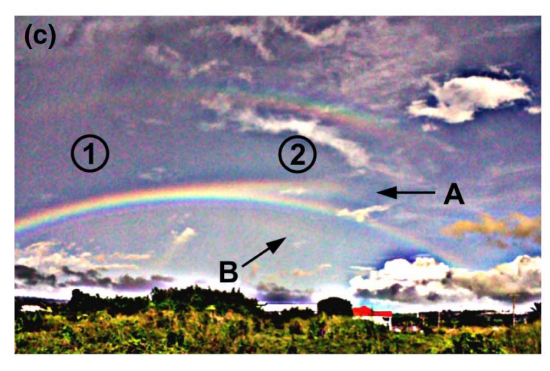


Fig. 5. (a) Triple-split rainbow photographed 5 August 2012, 18:24 JST at Yobuko, Kyushu island, Japan, by Kunihiro Tashima ($h_S = 9.7^{\circ}$). For orientation, the arrow indicates the intersection point of the 138° small circle (measured from the Sun, corresponding to the familiar "rainbow size" value of 42° from the antisolar point) with the right edge of the image. (b) Inhomogeneous split rainbow photographed 18 November 2009, 15:17 AST at Bridgetown, Barbados, by Mark Worme ($h_S = 28.3^{\circ}$); (c) unsharp masked and contrast enhanced version of (b), with labels indicating the upper branch (A), recently found lower branch (B), celestial region of conventional rainbow appearance (1) and region of split appearance of the primary (2).

distribution according to Eq. (9), which I chose to represent the standard case, just results in standard rainbows without any sign of splitting. It turned out to be necessary to assign higher amplitudes to smaller drops ($a_0 \approx 0.3$ mm) in order to split the primary and move the upper branch into the dark band, e.g., by the following amplitude distribution:

$$A_{2,0}^* = 0.025 \cdot \left(\frac{a_0}{1 \text{ mm}}\right)^{0.556}$$
 (13)

When doing so, the two shifted branches appear in the simulation, but there is yet no central arc. This situation might indeed be typical for some twinned rainbow displays with widely separated primaries of almost identical appearance [71]. My first attempt at including the central branch was the implementation of a cutoff size for the oscillations, inspired by the field measurements [21], but at a lower threshold. This would allow enough of the smaller, nonoscillating drops to create the central branch. However, I achieved no satisfying results this way. As an alternative, I assumed a mixture between oscillating and nonoscillating drops, i.e., a bimodal distribution. Due to the nonlocal nature of the eDSOD, this can be realized in nature by spatial inhomogeneities, e.g., by looking through a veil of oscillating drops into a shower of nonoscillating ones.

The hypothesis of such inhomogeneous oscillation distributions is further supported by the reanalysis of an older photograph that aroused much speculation some years ago [Fig. 5(b)] [72,73]. After unsharp masking and contrast enhancement [Fig. 5(c)], not only the strong upward branch A is visible, but also a weak and more diffuse downward branch B. The latter seems to have been overlooked in earlier discussions of this photograph. In the context of drop oscillations, it is possible to interpret the changes in the primary's manifestation as caused by an onset of oscillations from region 1 to region 2, i.e., effectively a similar situation as proposed for Fig. 5(a), but in this case seen from the side.

Figure 6 shows the results of several attempts to simulate Fig. 5(a). In Fig. 6(a), only oscillating drops with monodisperse amplitudes and perfectly nonoscillating drops, both at zero tilts, were used. The result matches the photograph acceptably well, though there are deviations near the coalescence point of the branches. These might be due to a residual lateral component of the spatial oscillation inhomogeneities or the presence of other modes than (2,0). For Fig. 6(b), the oscillation properties of both components were blurred to some degree, i.e., a Gaussian distribution was assigned to the oscillation branch, and the previously nonoscillating drops were given amplitudes following an exponential distribution. Additionally, tilts were switched on. This results in a reduced definition of the individual rainbow branches, but they are still recognizable and could easily be enhanced by standard image processing.

For comparison, I also included simulations based on nonoscillating drops and additional peaks in the eDSD, as previously used for twinned rainbows [9,10,64], shown in Fig. 6(c) (zero tilts) and 6(d) (tilts switched on). When comparing Figs. 5(a) and 6(c), it is obvious that this model does not reproduce the correct branch positions, as clearly visible from the arrow positions (indicating the intersection points of the traditional rainbow angle and the right edge of the simulation image). Moreover, the lowest branch seems to be completely wiped out by the tilts [Fig. 6(d)]. This is likely due to the fact that it occurs at the greatest distance from the sphere drop rainbow's circle, i.e., these drops are more distorted than those of any other category, including the extremal elongations in Fig. 6(b). The higher the deviation from a spherical shape, the more effective the blurring effect of tilts will be. In consequence, the oscillation model clearly provides a better fit to the observation than the multipeaked eDSD.

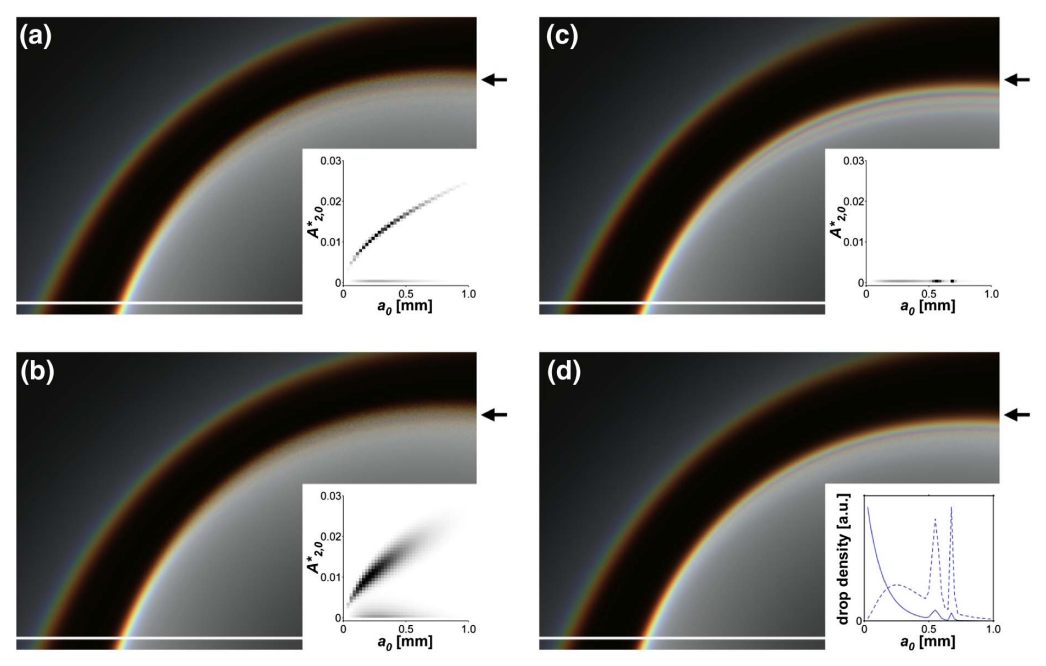


Fig. 6. DMK simulations corresponding to Fig. 5(a) for various parameter combinations, based on a $\mu=0$, $\Lambda=4$ mm⁻¹ eDSD. (a) Mixture of 83 % drops with monodisperse (2,0) amplitudes following Eq. (13) and 17% nonoscillating drops, zero tilts; inset, corresponding CS-eDSOD; (b) mixture of 83% drops with Gaussian polydisperse (2,0) amplitudes following Eq. (13), $\sigma_{\rm rel}=0.15$, and 17% drops with exponentially distributed amplitudes, scaling parameter (expected value) 0.002, Gaussian tilts $\sigma=7^\circ$; inset, corresponding CS-eDSOD; (c) nonoscillating drops, two narrow peaks centered at $a_0=0.55$ mm and $a_0=0.68$ mm added to the eDSD [64], zero tilts; inset, corresponding CS-eDSOD; (d) same as (c), but with Gaussian tilts $\sigma=7^\circ$; inset, corresponding eDSD (solid line) and CS-eDSD (dashed line, shows identical information as inset in (c). As in Fig. 5(a), the arrow indicates the position along the right image edge at which the scattering angle amounts to 138°.

4. CONCLUSIONS

Natural rainbows are much more complicated than might be expected, and their accurate modeling is a challenging and ongoing task. The present simulation study reports on the inclusion of the BC drop shape model, (2,0) oscillations, axis tilts, and rainbow orders up to the seventh in geometric-optical calculations, as well as including such oscillations and tilts in Möbius shifts to be applied to Debye series data for the primary and secondary rainbow. The main results are:

- 1) If a rain shower contains a noteworthy portion of larger drops ($a_0 > \approx 0.8$ mm), new features in the form of bright spots in the Sun's vertical may appear. These can be attributed to specific rainbow orders, though they are dislocated from the respective (near)spherical drop rainbow. The reasons for their comparatively high intensities are the onset of caustic involution at certain critical drop sizes, which under this condition will be present in the eDSD; and (multiple) total internal reflections. Unfortunately, most of the spots are either located below the horizon or are embedded in the bright forward-scattering disc. Though they are stable against drop shape variations in broad eDSDs and (2,0) oscillations, moderate tilts tend to blur them and may render them unrecognizable.
- 2) (2,0) oscillations can provide an explanation for rare triple-split primary rainbows. This is facilitated through a selection effect for near-extremal states due to the vanishing oscillation velocity at these points. Thus, a single drop size contributes with two effective shapes to the rainbow, and

for smaller drops one of the extremal states can obtain an elongated shape. This explains why one of the primary branches can be shifted towards the secondary, i.e., in the opposite direction of the Möbius shift for oblate drops. Consequently, attempts at reconstructing eDSDs from rainbow photographs should take oscillations into account. Furthermore, a set of nonoscillating or weakly oscillating drops is necessary to create the center branch. A possible scenario for this is spatially separated sets of drops along the line of sight. The result is stable against moderate spreads of oscillation amplitudes and moderate tilts.

Other researchers have undertaken extensive efforts to investigate the dominant oscillation modes, amplitudes, and tilt angles in natural rainfall, mostly with the aim of increasing the accuracy of rainfall rate measurements by radar backscattering methods [20,32]. However, the results reveal a rather complex and variable picture. For rainbow simulations, this means that there are many degrees of freedom in the modeling, and especially for rare phenomena, the input parameters—the effective drop size and oscillation distribution, as well as the distribution of tilts—have to be guessed. So far, I did not attempt to solve the inverse problem by iterative modeling.

For future simulations, it seems worthwhile to test the other relevant oscillation modes ((2,1), (2,2), and (3,1)), as well as to check the influence of updated equilibrium shape models [74,75]. A deeper study of the caustic evolution for realistic drop shapes and various light incidence directions is an interesting topic from the theoretical point of view. The Möbius

shift database can also be extended to more accurate models beyond the present 2HS and incorporate dispersion and intensity variations. This would allow one to exhaust the full potential of the shift approach. Finally, I want to suggest that observers pay attention to any dynamic events that might synchronize drop oscillations or affect the tilts during a rainbow displaylightning, thunder, or aircraft shockwaves. It seems strange that there are only few old observations [8], while the probably related phenomenon of "moving ripples" in halos and cloud iridescence is comparatively well documented [76].

Acknowledgment. I wish to thank Kunihiro Tashima, Liu Hai-Cheng, and Mark Worme for sending me their rainbow photographs, permitting me to use them in my publications and patiently answering my questions concerning the details of their observations. I also want to express my gratitude to Ji Yun for organizing communication and translations, and Günther Können for his help in accessing older meteorological observations from the Netherlands.

Disclosures. The author declares no conflicts of interest.

REFERENCES AND NOTES

- J. A. Adam, "The mathematical physics of rainbows and glories," Phys. Rep. 356, 229–365 (2002).
- C. B. Boyer, The Rainbow: from Myth to Mathematics (Yoseloff, 1959), pp. 159–160 and 223–224.
- J. A. Lock and G. P. Können, "Rainbows by elliptically deformed drops. I. Möbius shift for high-order rainbows," Appl. Opt. 56, G88–G97 (2017).
- W. Möbius, "Zur Theorie des Regenbogens und ihrer experimentellen Prüfung," Abh. Kgl. Sächs. Ges. Wiss. Math.-Phys. Kl. 30, 108–254 (1907).
- 5. A. B. Fraser, "Why can the supernumerary bows be seen in a rain shower?" J. Opt. Soc. Am. **73**, 1626–1628 (1983).
- G. P. Können and J. A. Lock, "Rainbows by elliptically deformed drops. II. The appearance of supernumeraries of high-order rainbows in rain showers," Appl. Opt. 56, G98–G103 (2017).
- 7. G. P. Können, "Appearance of supernumeraries of the secondary rainbow in rain showers," J. Opt. Soc. Am. A 4, 810–816 (1987).
- F. E. Volz, "Some aspects of the optics of the rainbow and the physics of rain," in *Physics of Precipitation*, H. Weickmann, ed., Geophysical Monograph 5 (American Geophysical Union, 1960), pp. 280–286.
- A. Haußmann, "Observation, analysis, and reconstruction of a twinned rainbow," Appl. Opt. 54, B117–B127 (2015).
- A. Haußmann, "Polarization-resolved simulations of multiple-order rainbows using realistic raindrop shapes," J. Quant. Spectrosc. Radiat. Transfer 175, 76–89 (2016).
- J. A. Lock, "Supernumerary spacing of rainbows produced by an elliptical-cross-section cylinder. I. Theory," Appl. Opt. 39, 5040–5051 (2000).
- C. L. Adler, D. Phipps, K. W. Saunders, J. K. Nash, and J. A. Lock, "Supernumerary spacing of rainbows produced by an ellipticalcross-section cylinder. II. Experiment," Appl. Opt. 40, 2535–2545 (2001).
- K. Sassen, "Angular scattering and rainbow formation in pendant drops," J. Opt. Soc. Am. 69, 1083–1089 (1979).
- P. L. Marston and E. H. Trinh, "Hyperbolic umbilic diffraction catastrophe and rainbow scattering from spheroidal drops," Nature 312, 529– 531 (1984).
- H. J. Simpson and P. L. Marston, "Scattering of white light from levitated oblate water drops near rainbows and other diffraction catastrophes," Appl. Opt. 30, 3468–3473 (1991).

- D. S. Langley and P. L. Marston, "Generalized tertiary rainbow of slightly oblate drops: observations with laser illumination," Appl. Opt. 37, 1520–1526 (1998).
- A. Haußmann, "Light scattering from sessile water drops and raindrop-shaped glass beads as a validation tool for rainbow simulations," Appl. Opt. 56, G136–G144 (2017).
- T. Nousiainen and K. Muinonen, "Light scattering by Gaussian, randomly oscillating raindrops," J. Quant. Spectrosc. Radiat. Transfer 63, 643–666 (1999).
- 19. T. Nousiainen, "Scattering of light by raindrops with single-mode oscillations," J. Atmos. Sci. **57**, 789–802 (2000).
- M. Szakáll, S. K. Mitra, K. Diehl, and S. Borrmann, "Shapes and oscillations of falling raindrops—a review," Atmos. Res. 97, 416–425 (2010).
- K. V. Beard, R. J. Kubesh, and H. T. Ochs, III, "Laboratory measurements of small raindrop distortion. Part I: Axis ratios and fall behavior," J. Atmos. Sci. 48, 698–710 (1991).
- K. V. Beard and R. J. Kubesh, "Laboratory measurements of small raindrop distortion. Part 2: Oscillation frequencies and modes," J. Atmos. Sci. 48, 2245–2264 (1991).
- T. Timusk, "Flashes of light below the dripping faucet: an optical signal from capillary oscillations of water drops," Appl. Opt. 48, 1212–1217 (2009).
- http://dl.meteoros.de/haussmann/AHaussmann_DisTripRainbows_ supp_inf.pdf.
- 25. L. Cowley, "Anomalous bows," http://atoptics.co.uk/fz845.htm.
- A. Haußmann, "Triple-split rainbow observed and photographed in Japan, August 2012," https://atoptics.wordpress.com/2015/03/ 11/triple-split-rainbow-observed-and-photographed-in-japanaugust-2012/.
- A. Boonsinsuk, "Triple-split rainbow," (in Thai language) http://www.cloudloverclub.com/triple-spit_rainbow-chiang_dao/.
- A. Haußmann, "A multi-split rainbow from south-east China, August 12th, 2014," https://atoptics.wordpress.com/2019/06/27/a-multi-split-rainbow-from-south-east-china-august-12th-2014/.
- S. D. Gedzelman, "Rainbows in strong vertical electric fields," J. Opt. Soc. Am. A 5, 1717–1721 (1988).
- F. Pattloch and E. Tränkle, "Monte Carlo simulation and analysis of halo phenomena," J. Opt. Soc. Am. A 1, 520–526 (1984).
- V. N. Bringi, M. Thurai, and D. A. Brunkow, "Measurements and inferences of raindrop canting angles," Electron. Lett. 44, 1425–1426 (2008).
- G.-J. Huang, V. N. Bringi, and M. Thurai, "Orientation angle distributions of drops after an 80-m fall using a 2D video disdrometer," J. Atmos. Ocean. Technol. 25, 1717–1723 (2008).
- R. L. Lee, "Mie theory, Airy theory, and the natural rainbow," Appl. Opt. 37, 1506–1519 (1998).
- S. D. Gedzelman, "Simulating rainbows in their atmospheric environment," Appl. Opt. 47, H176–H181 (2008).
- S. Kanamori, K. Fujiwara, T. Yoshinobu, B. Raytchev, T. Tamaki, and K. Kaneda, "Physically based rendering of rainbows under various atmospheric conditions," in 18th Pacific Conference on Computer Graphics and Applications (2010).
- I. Sadeghi, A. Munoz, P. Laven, W. Jarosz, F. Seron, D. Gutierrez, and H. W. Jensen, "Physically-based simulation of rainbows," ACM Trans. Graph. 31, 1–12 (2012).
- P. Laven, "Supernumerary arcs of rainbows: Young's theory of interference," Appl. Opt. 56, G104–G112 (2017).
- P.-E. Ouelette, "Supernumerary bows: caustics of a refractive sphere and analysis of the relative overall Gouy phase shift of supernumerary rays," Appl. Opt. 58, 712–722 (2019).
- 39. A corrected version of the supporting information discussing the mathematical details of the simulation is linked in [17].
- S. D. Gedzelman, "Rainbow brightness," Appl. Opt. 21, 3032–3037 (1982).
- H. E. Edens and G. P. Können, "Probable photographic detection of the natural seventh-order rainbow," Appl. Opt. 54, B93–B96 (2015).
- G. P. Können, "Polarization and visibility of higher-order rainbows," Appl. Opt. 54, B35–B40 (2015).
- Y. P. Han, L. Méès, K. F. Ren, G. Gouesbet, S. Z. Wu, and G. Gréhan, "Scattering of light by spheroids: the far field case," Opt. Commun. 210, 1–9 (2002).

- F. Xu, J. A. Lock, and C. Tropea, "Debye series for light scattering by a spheroid," J. Opt. Soc. Am. A 27, 671–686 (2010).
- J. A. Lock, C. L. Adler, B. R. Stone, and P. D. Zajak, "Amplification of high-order rainbows of a cylinder with an elliptical cross section," Appl. Opt. 37, 1527–1533 (1998).
- C. L. Adler, J. A. Lock, and B. R. Stone, "Rainbow scattering by a cylinder with a nearly elliptical cross section," Appl. Opt. 37, 1540–1550 (1998).
- H. R. Pruppacher and R. L. Pitter, "A semi-empirical determination of the shape of cloud and rain drops," J. Atmos. Sci. 28, 86–94 (1971).
- K. V. Beard and C. Chuang, "A new model for the equilibrium shape of raindrops," J. Atmos. Sci. 44, 1509–1524 (1987).
- C. C. Chuang and K. V. Beard, "A numerical model for the equilibrium shape of electrified raindrops," J. Atmos. Sci. 47, 1374–1389 (1990).
- 50. In [9], the value for the parameter f_3 in Eq. (5) was given mistakenly without its minus sign, i.e., it should read correctly $f_3 = -0.2911$.
- E. Becker, W. J. Hiller, and T. A. Kowalewski, "Experimental and theoretical investigation of large-amplitude oscillations of liquid droplets," J. Fluid Mech. 231, 189–210 (1991).
- A. Prosperettia, "Linear oscillations of constrained drops, bubbles, and plane liquid surfaces," Phys. Fluids 24, 032109 (2012).
- 53. For real-valued spherical harmonics, m>0 modes have a $\cos(m\,\varphi)$ dependence, while the ones with m<0 have a $\sin(m\,\varphi)$ dependence. These are linearly independent, and both are necessary to build the complete basis function set. However, they can be arithmetically combined to a single m>0 mode in a rotated (and depending on the phase offsets, possibly rotating) coordinate system. Moreover, in video disdrometer measurements, only a projection of the drop surface is seen. This explains why most papers on drop oscillations neglect modes with negative m.
- J. Q. Feng and K. V. Beard, "A perturbation model of raindrop oscillation characteristics with aerodynamic effects," J. Atmos. Sci. 48, 1856–1868 (1991).
- 55. M. Szakáll, S. Kessler, K. Diehl, S. K. Mitra, and S. Borrmann, "A wind tunnel study of the effects of collision processes on the shape and oscillation for moderate-size raindrops," Atmos. Res. **142**, 67–78 (2014)
- S. Müller, M. Szakáll, S. K. Mitra, K. Diehl, and S. Borrmann, "Shapes and oscillations of raindrops with reduced surface tensions: measurements at the Mainz vertical wind tunnel," Atmos. Res. 119, 38–45 (2013).
- 57. H. R. Pruppacher and J. D. Klett, *Microphysics of Clouds and Precipitation*, 2nd ed. (Kluwer Academic, 1997), pp. 400–408.
- 58. For the (2,0) mode, the temporally averaged axis ratio corresponds to the axis ratio of the nonoscillating equilibrium state. This is not necessarily the case for $m \neq 0$ modes.
- K. V. Beard and A. R. Jameson, "Raindrop canting," J. Atmos. Sci. 40, 448–454 (1983).
- M. Agrawal, A. R. Premlata, M. K. Tripathi, B. Karri, and K. C. Sahu, "Nonspherical liquid droplet falling in air," Phys. Rev. E 95, 033111 (2017).
- M. Balla, M. K. Tripathi, and K. C. Sahu, "Shape oscillations of a nonspherical water droplet," Phys. Rev. E 99, 023107 (2019).

- C. W. Ulbrich, "Natural variations in the analytical form of the raindrop size distribution," J. Clim. Appl. Meteorol. 22, 1764–1775 (1983).
- 63. The raw RGB simulation images were subjected to a gamma increase (to $\gamma=2$) (Figs. 3,4, and 6) and a subsequent contrast enhancement (Figs. 3 and 4) before display. No artificial background was added to the simulations.
- 64. The actual eDSD for these calculations is given by the formula $n(a_0)=n_0\cdot\exp(-2\cdot a_0\cdot \Lambda)+n_1\cdot\exp(-(a_0-a_1)^2/2\sigma_1^2)+n_2\cdot\exp(-(a_0-a_2)^2/2\sigma_2^2)$ and this set of parameters: $n_0=1$ (normalization factors and actual physical units are not relevant), $\Lambda=4$ mm⁻¹, $n_1=0.066, a_1=0.55$ mm, $\sigma_1=0.025$ mm, $\sigma_2=0.06, a_2=0.68$ mm, $\sigma_2=0.01$ mm.
- 65. They can, however, be relevant for artificial-light rainbows, and maybe for reflection bows.
- M. Theusner, "Photographic observation of a natural fourth-order rainbow," Appl. Opt. 50, F129–F133 (2011).
- M. Großmann, E. Schmidt, and A. Haußmann, "Photographic evidence for the third-order rainbow," Appl. Opt. 50, F134–F141 (2011).
- 68. There is one older observation of a red spot appearing inside the primary rainbow above the antisolar point, recorded 20 September 1896, in Vlissingen, Netherlands, at a Sun elevation of about 13.3°. The elevation of the spot above the horizon was roughly estimated to be 14.5°, and it was interpreted as a reflected-light glory by the observer [69]. However, at this Sun elevation, no such spot does appear in the current simulations based on the BC model.
- 69. Koninklijk Nederlandsch Meteorologisch Instituut. Onweders, Optische Verschijnselen, Enz. in Nederland. Naar vrijwillige waarnemingen in 1896, Deel 17 (Amsterdam, 1897), pp. 48–49.
- 70. I am aware of only one single photograph showing a candidate twinned secondary rainbow (with the splitting point shifted off the center to the right), but more details concerning the observation and photographic equipment are needed for a definite assessment. It should be noted that modern cellphone and other digital cameras can produces artifacts when several frames are combined by an optimization algorithm, and the camera orientation was not kept fixed during the multiexposure.
- L. Cowley and T. Wooten, "Puzzling triple rainbow," https://www.atoptics.co.uk/fza149.htm.
- C. Hinz and M. Worme, "Twinned rainbow," https://atoptics. wordpress.com/2011/05/27/twinned-rainbow-2/.
- L. Cowley and M. Worme, "Peculiar rainbows," https://www.atoptics.co.uk/fz517.htm.
- J. Q. Feng and K. V. Beard, "Raindrop shape determined by computing steady axisymmetric solutions for Navier-Stokes equations," Atmos. Res. 101, 480–491 (2011).
- J. Appleyard, "Computational simulation of freely falling water droplets on graphics processing units," Ph.D. dissertation (School of Engineering, Cranfield University, 2013).
- C. Hinz, "Moving ripples," https://www.meteoros.de/themen/halos/ arbeit-des-akm/moving-ripples/.